diffusion-fundamentals.org
The Open-Access Journal for the Basic Principles of Diffusion Theory, Experiment and Application

Miniature mobile NMR sensors for material testing and moisture-monitoring

D. Oligschläger[1], K. Kupferschläger[1], T. Poschadel[1], J. Watzlaw[2], B. Blümich[1]

[1]Institut für Technische und Makromolekulare Chemie (ITMC), RWTH Aachen University, Worringer Weg 1, 52074 Aachen, Germany

[2]Institut für Werkstoffe der Elektrotechnik 1 (IWE 1), RWTH Aachen University, Sommerfeldstraße 24, 52074 Aachen, Germany

Corresponding author: Dirk Oligschläger, Institut für Technische und Makromolekulare Chemie (ITMC), RWTH Aachen University, Worringer Weg 1. 52084 Aachen, Germany,

E-Mail: oligschlaeger@itmc.rwth-aachen.de

Abstract

Miniaturization plays an essential role in modern life of the 21st century. It is encountered, e.g., in communication, personalized and portable computers and in medicine. Miniaturization also affects NMR, one of the most versatile analytical tools, leading to dedicated sensors and portable devices which lead to new applications of NMR in different disciplines. The miniaturization of two portable stray-field NMR sensor types, the NMR-MOUSE® and an inside-out sensor are reported in this work. The sensors are critically evaluated and compared to other standard probes. Applications in material testing and civil engineering are evaluated.

Keywords

NMR stray-field sensors, Miniaturization, NMR of rigid materials, Inside-out NMR, Civil Engineering

1. Introduction

Nuclear-Magnetic-Resonance (NMR) is a physical phenomenon based on the principle of exciting nuclear spins with radiofrequency pulses, the frequency of which matches the Larmor frequency of the nuclear spins. This principle has been applied in many different research fields such as chemical structure analysis, materials testing and in medicine. To access certain nuclear spins via radiofrequency pulses, the nuclei have to be exposed to a magnetic field [1]. These magnetic fields can be classified as high and low. Low magnetic fields as created by permanent magnets can yield magnetic field strengths up to 85 MHz proton Larmor frequency, whereas superconducting high field magnets reach drastically higher field strengths [2]. Magnetic fields can either be produced by currents running through wires of a certain resistance and through superconducting media or by the use of permanent magnets.

The development of compact NMR devices started with the use of permanent magnets in well-logging sensors of the inside-out type [3]. The first widely used logging-sensors are known as the Jackson-tool [3,4], the NUMAR tool [5] and a sensor developed by Schlumberger [6,7]. Whereas the latter is meant to be a sweet-spot sensor, the first geometries detect the NMR signal from a circular ring or a cylindrical shell [5,7]. Besides inside-out magnet geometries also other magnet designs have been developed. They can be divided into single-sided magnets like the NMR-MOUSE® and closed magnets like the Halbach magnet [8]. Both sensor types are referred to be low-field NMR sensors and incorporate highly inhomogeneous magnetic fields when compared to superconducting high field magnets. To compensate for field inhomogeneities, echo detection methods are applied. All sensor types are well-suited for relaxation and diffusion measurements.

Single-sided NMR sensors detect the NMR signal from a sensitive volume or slice located outside the magnet assembly. Today most single-sided sensors in use are similar in design to the NMR-MOUSE®. They are being used for relaxometry, diffusometry and 1D-imaging in terms of depth profiling. Related devices that have to mentioned in this context are the GARFIELD magnet and other stray-field sensors like the barrel magnet and the NMR-MOLE (**MO**bile **L**ateral **E**xplorer) [8].

The developments in low-field NMR of the last five years clearly aim at shrinking the NMR tools for applications in personalized medicine [9,10], life science [9,10] and for building science [11,12]. Both, the magnets itself as well as the radiofrequency coil including NMR electronics are being miniaturized. Focusing on existing sensors with MOUSE geometry, we

diffusion-fundamentals.org 22 (2014) 8, pp 1-25

present a considerably smaller sensor of the NMR-MOUSE® type (Micro-MOUSE) with a weight reduction of 99 % and a volume reduction of 98 % compared to a conventional NMR-MOUSE® with 5 mm depth access. This sensor is combined with a micro-structured radiofrequency coil with dimensions of 2 x 2 mm^2 [13]. Applications range from depth profiling of thin layers up to measurements of extremely hard polymers, where short echo times in multi-echo trains lead to an increase of signal from rigid material components and a higher number of acquired data points. In the present study we discuss these effects by example of the curing of acrylic paint.

An example for use of a single-sided NMR sensor applied to a civil engineering topic was developed by Cano-Barrita et al. who presented an NMR disk of 30 mm in diameter and 12 mm in height to measure hydration processes in cement [11]. The measurement frequency is 10.2 MHz and the used echo times are in the range of 160 μs. The main advantages of such a sensor are the low costs and the possibility to permanently embed it into the cement material. The size-reduction of single-sided NMR sensors such as the Micro-MOUSE is a trade off between beneficial short echo times, the possibility to resolve thin layers with fast relaxation components, to measure very small structural details, improved portability and disadvantages like a limited depth range, a lower absolute signal-to-noise ratio due to smaller sample volume and a considerably higher gradient.

Miniaturized inside-out sensors can be used in the field of hydrology and building science. Examples are the Slim-Line-Logging tool for relaxation and diffusion measurements in soil [14]. The sensor consists of a dumbbell shape magnet assembly with a polarization transverse to its long axis, creating an ideal dipolar magnetic field. The radiofrequency coil was recently optimized [15] to enable signal detection from a cylindrical shell compared to the single-sided fashion of the first Slim-Line-Logging tool [14]. In this study we also present a miniaturized sensor of similar design, the DIP (Direct Insertion Probe) stick sensor for moisture analysis in building materials.

2. Miniature single-sided NMR sensor for material testing – The Micro MOUSE

2.1. General aspects

In this work we reduced the size of the standard state-of-the-art NMR-MOUSE® [16,17] with 5 mm depth access (PM5) drastically, by using four magnet cubes each with a volume of 1 x 1 x 1 cm^3 while keeping the NMR frequency of 17 MHz on the same level. The reason was simply to reduce sensitivity losses which naturally occur when reducing the sensor size, due to a smaller sensitive volume and consequently a smaller number of detectable spins. It has to be noticed, that these size considerations already include the NMR circuit, consisting of two variable non-magnetic capacitors and an SMB connector. The size-reduction affects two other key parameters. The distance of the sensitive slice from the magnet surface at a frequency of 17 MHz is considerably reduced. While the sensitive volume of the PM5 NMR-MOUSE® is located 5 mm above the rf coil, the depth access of the Micro-MOUSE is restricted to a measurement depth of 0.2 mm. A parameter that changes with decreasing size of the MOUSE magnets, is the gradient. The gradient describes the change of the magnetic field at a certain position in space. Per definition it is the first spatial derivative of the magnetic field strength. For single-sided devices it is commonly determined by measuring a sample with known self-diffusion coefficient, such as ultrapure water ($D = 2.3 \cdot 10^{-9} m^2 s^{-1}$) and varying the echo time within a CPMG pulse sequence. The gradient can be calculated according to equation (4) from the slope of a linear fit when plotting $1/T_{2eff}$ versus t_E^2. For the Micro-MOUSE a value of 107.6 T/m was determined (Fig. 1 e). The present gradient of the Micro-MOUSE is 4.9 × higher than the gradient (22 T/m) of a standard Profile NMR-MOUSE® (PM5) with 5 mm depth access. When comparing the gradient of different MOUSE® sensors, a strong dependence of the size dimension (surface area of the magnet assembly) and the depth access can be found (Fig. 1 f) As a rule of thumb there is an exponential dependence of the depth access as well as the surface area of MOUSE sensors and their magnetic field gradient (Fig. 1 f). The gradient variation goes ahead with a change in the thickness of the sensitive slice. The excitation bandwidth Δf_{exc} is directly dependent on the gradient strength G_0 and both define the resolution Δz [7]:

$$\Delta z = \frac{\Delta f_{exc}}{\gamma G_0} \qquad (1)$$

The achievable spatial resolution for single-sided NMR sensors, such as the NMR-MOUSE®, depends on the measurement technique. In the context of this work the term *resolution* refers to the one-dimensional *depth resolution*. Depth profiles can either be obtained in single-shot

experiments in terms of the Fourier transform of the echo shape [18], or in multiple experiments by shifting the sensitive slice through the sample with a motor lift [19]. The narrower the sensitive slice, the higher is the spatial resolution. When using an automated lift, the step-size of the lift typically is larger than the achievable resolution. Besides the gradient, the excited volume is proportional to the inverse of the pulse length. When comparing the signal-to-noise-ratio (SNR) of different NMR devices, the SNR values have to be normalized to the excited volume, considering the gradient and the pulse length as dominant parameters, when assuming the same pulse-shape.

Instead of hand wound copper coils, the use of micro-fabricated micro-coils [13] enables further miniaturization, improves sensitivity, and enables echo times as short as 10 μs. Short echo times are of benefit when analyzing materials with very short relaxation times such as semi-crystalline polymers, cementeous materials and dry paint. Consequently more data points can be recorded in the initial, fast relaxation regime compared to echo trains acquired with longer echo times [13], and, in particular, the definition of the rapidly decaying relaxation components is improved. The smaller micro-coil diameter reduces the size of the measurement spot to only 2 x 2 mm^2, while for instance the standard coil in the PM5 sensor averages the signal laterally over an area of 157 mm^2.

2.2 Results and discussion

2.2.1. Construction details

Permanent magnet cubes made of NdFeB with a magnetization grade of N52 (52 MGOe) and a volume of 1 cm^3 each, were positioned on an iron yoke of 0.5 cm thickness, with gaps g_b = 0.5 mm and g_s = 0.15 mm according to Fig. 1 a [16,17]. The micro-fabricated radiofrequency coil of 2 mm diameter, made of gold, consists of four layers with five turns each (Fig. 1 c) [13]. The coil is optimized for a measurement frequency of 17 MHz, and is positioned above the center of the magnet assembly in such a way, that the sensitive slice is located 0.2 mm above the surface of the coil, 4 mm away from the magnet surface as indicated in Fig. 1 d.

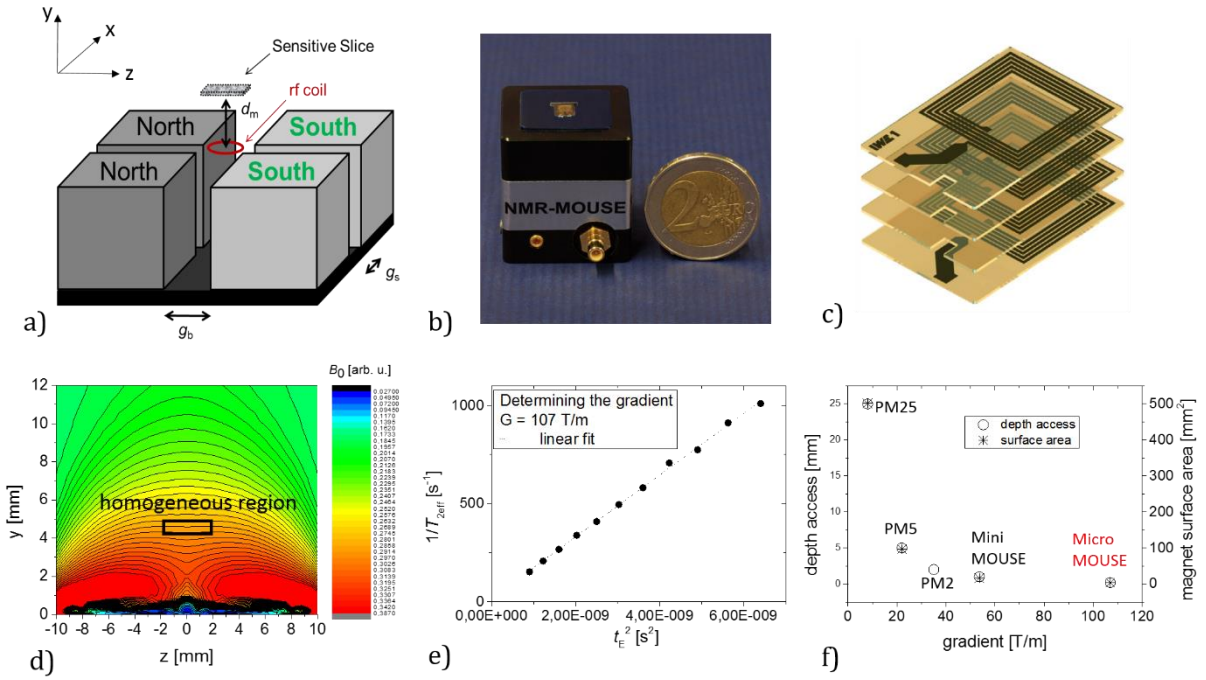

Fig. 1: a) Scheme of the NMR-MOUSE® set-up. Four magnet blocks are positioned on an iron yoke. The grey scale indicates the polarization direction of the magnets, also indicated by 'North' and 'South' referring to the magnet pole at the open surface. The inter-magnet gaps g_s and g_b are variables, as well as the magnet size. Depending on the magnet size and also the distance of the sensitive slice varies. b) Photograph of the Micro-MOUSE. c) Scheme of a micro-fabricated radiofrequency coil consisting of four layers with five turns each. The conducting material is gold [13]. d) Map of the static magnetic field B_0 according to the coordinate frame shown in a). The magnetic field was mainly optimized in terms of homogeneity. Since the highest magnetization grade N52 is not yet included in the software, only arbitrary units of the magnetic field are shown. Therefore the gradient has to be determined experimentally. d) Determination of the gradient according to equation (4). Ultrapure water was measured with the CPMG sequence by varying echo time. The gradient can be calculated from the slope of a linear fit, when plotting the inverse transverse relaxation times against t_E^2. f) Correlation of the depth access and the magnet surface area of different NMR-MOUSE sensors with the magnetic field gradient.

The electronic NMR circuit, consisting of a capacitor arranged in parallel to the inductor (tune) and another capacitor in series to the coil (match) is placed underneath the iron yoke to improve shielding and to reduce the impact of eddy currents. The connection to the spectrometer is provided by SMB connector. The NMR circuit is tuned to 17.1 MHz and matched to an impedance of 50 Ω. They weight of the complete sensor is 80 g and its dimensions 2.8 x 2.8 x 3.1 cm^3.

2.2.2. Comparison to other single-sided sensors

A key parameter when comparing NMR sensors is sensitivity. The experimental parameter reflecting the sensitivity of a NMR sensor is the signal-to-noise ratio (SNR). It can be defined as follows [13]:

$$SNR = \frac{\text{Sum of echoes}}{\sqrt{(\text{Variance of noise level}) \cdot (\text{Nr. of echoes}) \cdot (\text{Nr. of scans})}} \qquad (2)$$

When determining the SNR level it is important to use the same reference sample for all devices. In this case, a saturated aq. $CuSO_4$ solution was used. To assure a genuine comparison of the signal-to-noise ratio, the complete sensitive volume of each sensor has to be filled with the reference sample. A recycle delay of 16 s was used during CPMG experiments to allow complete recovery of the equilibrium magnetization after each CPMG echo train. The echo data were accumulated over 128 echoes with 64 scans. For all sensors an echo time of 100 µs was used with an acquisition frame of 8 µs. The data were fitted with a mono-exponential decay function (equation 3), describing the loss of transverse magnetization with time *t*, where A_0 is the signal amplitude extrapolated to time zero of the signal decay and $T_{2\text{eff}}$ denotes the effective transverse relaxation time, a time constant representing molecular mobility [1],

$$A(t)=A_0\cdot\exp\left(-\frac{t}{T_{2\text{eff}}}\right) \tag{3}$$

When comparing the CPMG echo trains from different NMR-MOUSE designs, large differences in the signal decays of $CuSO_4$ doped water are noted (Fig. 2). These are due to the dependence of the signal decay on B_0field inhomogeneity, represented in form of the gradient G_0 (equation 4), as well differences in B_1. Another effect that explains the deviations in the echo decays, measured with different sensors (Fig. 2), is, that in inhomogeneous magnetic fields the measured effective relaxation time $T_{2\text{eff}}$, is affected by T_2 and T_1 due to superposing coherence pathways of magnetization, which can partially be compensated by phase cycling [7].

$$\frac{1}{T_{2\text{eff}}}=\frac{1}{T_2}+\frac{\gamma^2G_0^2Dt_E^2}{12} \tag{4}$$

Therefore the echo amplitudes were summed according to equation 2, up to the echo located at a time of $1 \times T_{2\text{eff}}$. To extract a SNR level per echo, per scan, the corresponding values shown in Tab. 1 were considered.

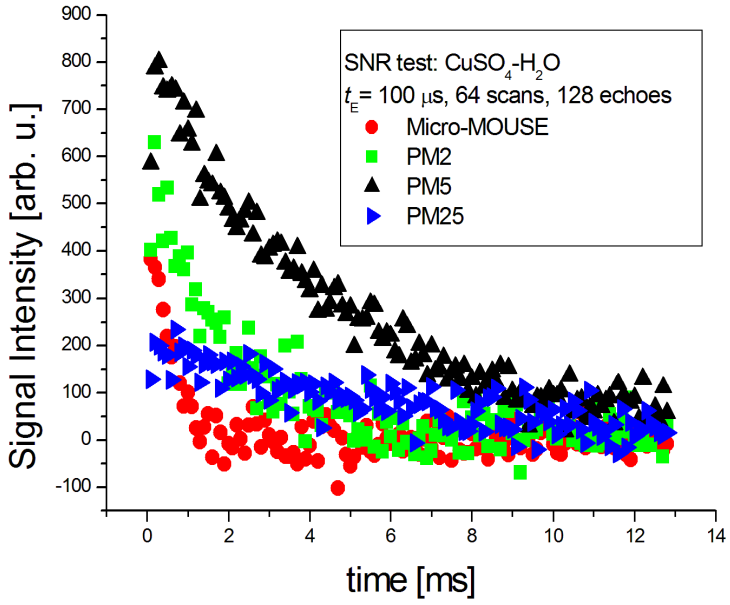

Fig. 2: Signal-to-noise (SNR) analysis of different single-sided NMR sensors of the Profile NMR-MOUSE® type. For calculation of the SNR the NMR signal was detected with a CPMG sequence. For each device the whole sensitive volume was immersed in aquaeous saturated $CuSO_4$ solution. The measurements were conducted with 64 scans, an echo time of 100 µs and 128 recorded echoes.

Tab. 1: Calculation of the signal-to-noise ratio per echo, per scan according to equation 2. In contrast to Tab. 2, absolute SNR values are shown.

Device	SNR (p.e., p.s.)	Noise-level	Sum of echoes	Echo Nr.
Micro-MOUSE	12.6	28.5	1201.3	5
PM 2	28.9	40.0	5667.2	15
PM 5	73.9	30.6	20689.8	40
PM 25	22.8	29.2	7904.9	64

At first glance, the SNR value of the Profile-MOUSE sensor with 5 mm depth access (PM5) seems to have the highest signal-to-noise ratio (Fig. 2 and Tab. 1). It is followed by the PM2, the PM25 and the Micro-MOUSE shows the lowest SNR per echo, per scan. For better comparison of the different sensors, the SNR was normalized to the excited volume, considering the gradient, the pulse length and the size of the coil, since obviously a larger coil detects a larger amount of spins. Considering these issues, the Micro-MOUSE shows a SNR level 2.8 times higher than the PM2 (Tab. 2). The lowest volume normalized signal-to-noise ratio is present in the Profile-MOUSE with 25 mm depth access. All sensors have different advantages and disadvantages. The PM5 sensor for instance, shows a lower volume-normalized signal-to-noise ratio than the Micro-MOUSE, but might be beneficial when analyzing samples with less spins, profiting from a higher *absolute* SNR (Tab. 1). A counter argument would focus on fast relaxation of samples with low amounts of spins. Here the Micro-MOUSE might profit

from small echo times such as 10 μs, and enables the recording of more data points in the fast relaxation regime as discussed in the following chapter.

Tab. 2: Calculation of the Signal-to-noise ratio per echo, per scan according to equation 1. The SNR values have been normalized to the excited sample volume, considering the excitation pulse length, the gradient and the lateral dimensions of the rf coil. The gradient values are obtained from the manufacturer Magritek and are checked with NMR measurements on ultrapure water and a variation of the echo time.

Device	**Gradient** [T/m]	**Pulse length** [μs]	**Coil surface** [mm^2]	**SNR** (p.e., p.s., normalized)
Micro-MOUSE	107	4	16	337
PM 2	35	3	25	122
PM 5	22	5	157	52
PM 25	8	22	982	4

2.2.3. Application: Tracking the drying of acrylic paint

As already discussed in the introduction and in the previous chapter, the use of micro-coils with a short dead time, 4 μs in our case, enables ultra-short echo times in CPMG sequences, such as 10 μs in minimum. This leads to an increase in the number of recorded echoes and consequently to an increase in information. This is essential when analyzing substances with short relaxation components such as semi-crystalline polymers, car-polish, cement and dry paint. With sensors that only allow the use of longer echo times, e.g. 50 μs as minimum echo time for the PM5 sensor it is hard to resolve fast relaxing components.

We show the beneficial use of short echo times by example of the drying process of acrylic paint. Studying the drying behavior of paint as well as the characterization of dry paint is of interest in many fields of research [20]. Paint is applied on buildings, furniture, vehicles and boats. Those substances are exposed to natural aging and degradation, and aging induced through environmental influences such as moisture, salts and aggressive contaminants such as tree resin and bird excrements [20]. This is why a non-invasive analytical methods such as single-sided NMR is of high interest to prevent, control and understand degradation processes.

For our investigations a layer of acrylic paint (blue; Cerulean Blue, Junghans Creativ, Acrylic Fine Quality) of 1 mm thickness was placed on a microscope glas slide of 150 μm thickness. The drying process was followed within a slice 950 μm away from the surface of the paint layer (Fig. 4 a). CPMG experiments were performed over a time of 1156 minutes with an acquisition time of 17 minutes for a single CPMG experiment. The experiment was carried out with an echo time of 20 μs and repeated with an echo time of 50 μs. 1300 and 500 echoes were recorded,

respectively, with a recycle delay of 1 s and a pulse length of 2.8 µs. The spectrometer was a KEA spectrometer from Magritek.

During the drying/hardening process of any kind of paint a reduction in molecular mobility is expected with an associated decrease of the T_{2eff} values obtained from NMR experiments. When paint dries, the solvent evaporates, which leads to an increase of the fast relaxing components when compared to the initial state of the fluid paint. We analyzed the CPMG data of the drying process with both, mono-exponential and bi-exponential fits. The residual values (R^2) show a much better data representation with bi-exponential fits (Fig 3 a). This becomes more pronounced with ongoing drying.

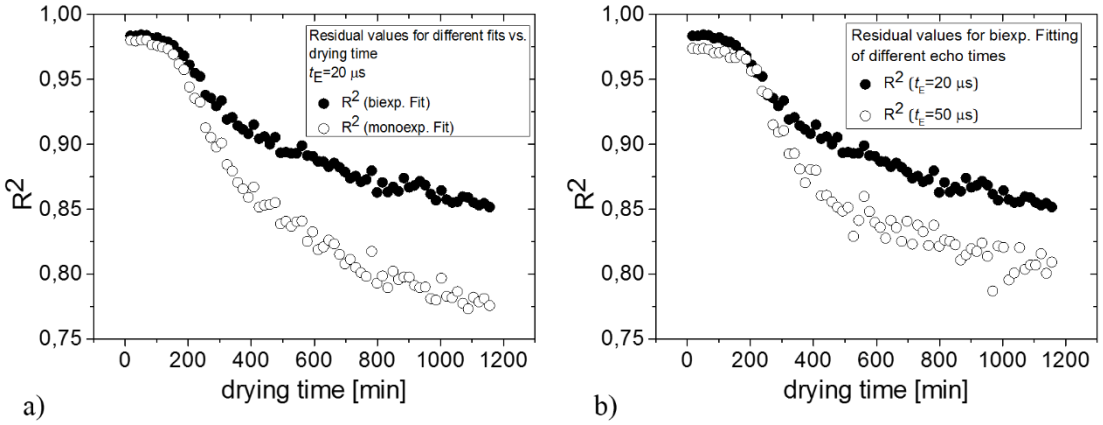

Fig. 3: a) Residual values for mono- and bi-exponential fits versus drying time. Each data point represents the fit residual from a single CPMG decay, measured at a certain drying time. At the beginning of the drying process both fit procedures show the same accuracy, while after a drying time of 200 minutes the bi-exponential fit describes the CPMG decay curves with higher accuracy. b) Comparison of residual values from bi-exponential fits of CPMG decays measured with different echo times. At the beginning of the drying process the fit quality is at the same level, while after a drying time of 200 minutes, the data quality measured with a short echo time is superior to the data set measured with a longer echo time.

The residual values also nicely show the benefits from using shorter echo times as shown in Fig. 3b. The residual values of a bi-exponential fit for the data set recorded with an echo time of 20 µs represents the data much better with ongoing drying time than with an echo time of 50 µs. This is due to a more accurate data description in the fast relaxation regime of already dry components.

The drying process itself can be monitored in different ways. A stable method that compensates for noise effects, is to plot mean values of a certain echo number of a CPMG decay versus drying time (Fig. 4 b). Integrating the complete CPMG echo decay with 1300 echoes produces to a T_2 weighted spin density. This data set leads to a delayed start of drying as can be seen in Figure 4 c, although the drying process starts significantly earlier. Such a T_2 weighted spin

density considers the molecular mobility stronger than the loss of solvent. This is why the beginning of the drying process can only be seen when molecules aggregate and change their mobility.

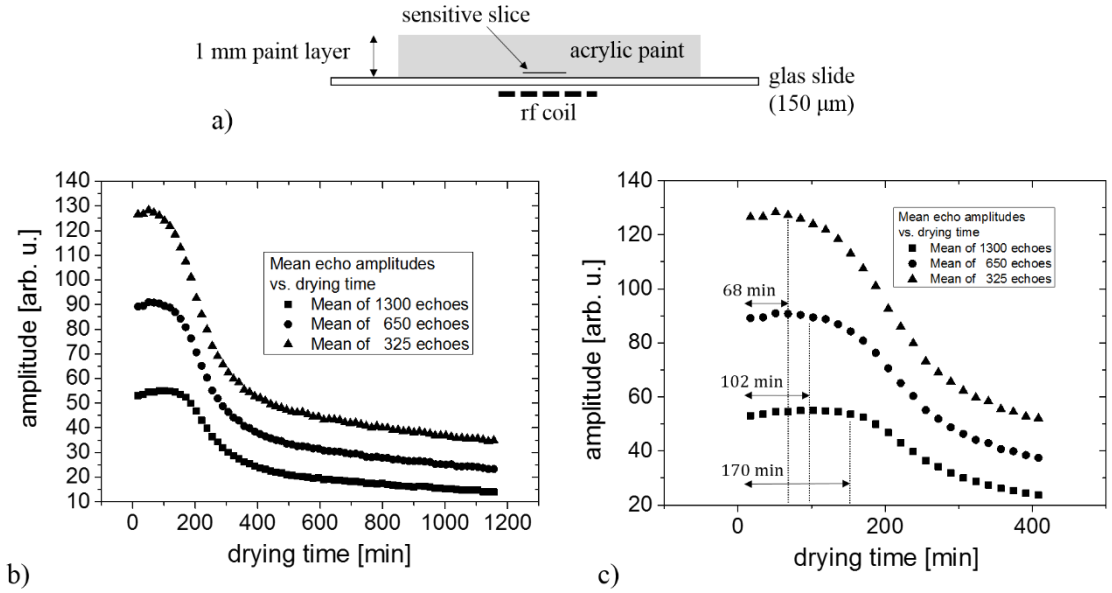

Fig. 4: a) Scheme of the measurement set-up. To assure reproducibility of the drying experiments, a layer of 1 mm acrylic paint was placed on a glas spacer and the drying process was followed with the micro-mouse. The sensitive slice was located 950 µm away from the initial paint surface. b) Drying of acrylic paint with time in terms of different CPMG contrasts. Each data point represents the integration of a certain echo amount. c) Zoom of the first part of the drying process shown in b). An echo integration over the complete CPMG decay leads to a T_2 weighted spin density, which results in significant differences in the drying plateau.

A more accurate, but also noise sensitive method is to plot the amplitudes for the short and the long relaxation components as well as the relaxation times versus the drying time. All parameters are extracted from bi-exponential fits. As is shown in Fig. 5 a, the relative amplitude of the long relaxation component (solvent) decreased with drying time, whereas the relative amplitude of the short component increases with time. The long component of the relaxation time firstly increases and then decreases as expected with hardening and evaporation of the solvent. The increase in T_{2long} at the beginning can be explained by a dominant diffusion term in the first drying period (equation 4). After a time of 220 minutes, T_2 becomes the dominant part, when a certain amount of solvent is already evaporated.

diffusion-fundamentals.org 22 (2014) 8, pp 1-25

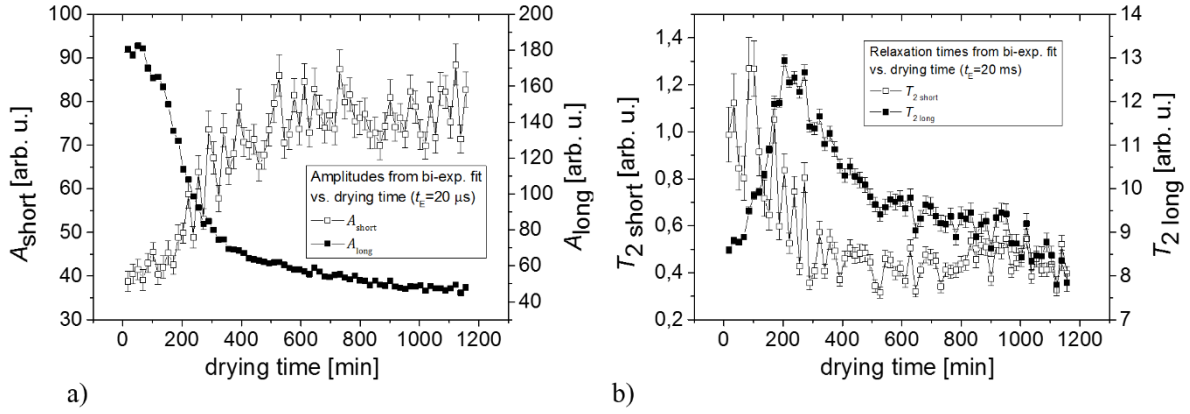

Fig. 5: a) Drying of acrylic paint with time, represented by the amplitudes obtained from a bi-exponential fit of CPMG data. Each data point represents the amplitude of a single CPMG echo train, measured at a certain drying time. b) Drying of acrylic paint with time, represented by the transverse relaxation times obtained from bi-exponential fits of the CPMG data. Each data point represents the short or long component of the relaxation time of a single CPMG echo train, measured at a certain drying time.

3. A miniaturized moisture sensor of the inside-out type

3.1. General Aspects

Moisture poses to be a major problem in early degradation to building materials. Standard analytical methods such as infrared thermography and electrical resistance sensors rely on indirect measurements which are often erroneous and needs time-consuming calibrations [12]. Thus, we introduce a miniaturized inside-out NMR sensor to directly detect moisture. A borehole tool called the 'DIP stick' (Direct Insertion Probe) was constructed, optimized and applied to monitor moisture dynamics in building materials with the ultimate goal of applying the tool in the field. This newly proposed tool can measure weak signals from any kind of construction material even in high-noise construction sites. The DIP stick is robust, inexpensive, mobile and light-weighted.

The principal design of the sensor is related to the NUMAR well logging sensor [5] and the Slim-Line-Logging tool [14, 15]. The signal is detected from a cylindrical shell, surrounding the magnet assembly (Fig. 6 a). The polarization transverse to the long axis of the cylindrical magnet creates a dipolar magnetic field B_0, whereas the oscillating, dipolar radiofrequency field, B_1, is created from a multi turn coil. The main differences of our proposed, miniaturized inside-out sensor, to the presented inside-out sensors presented in the introductory section are the considerably smaller size and a coil design which leads to smaller echo times, when using CPMG sequences.

diffusion-fundamentals.org 22 (2014) 8, pp 1-25

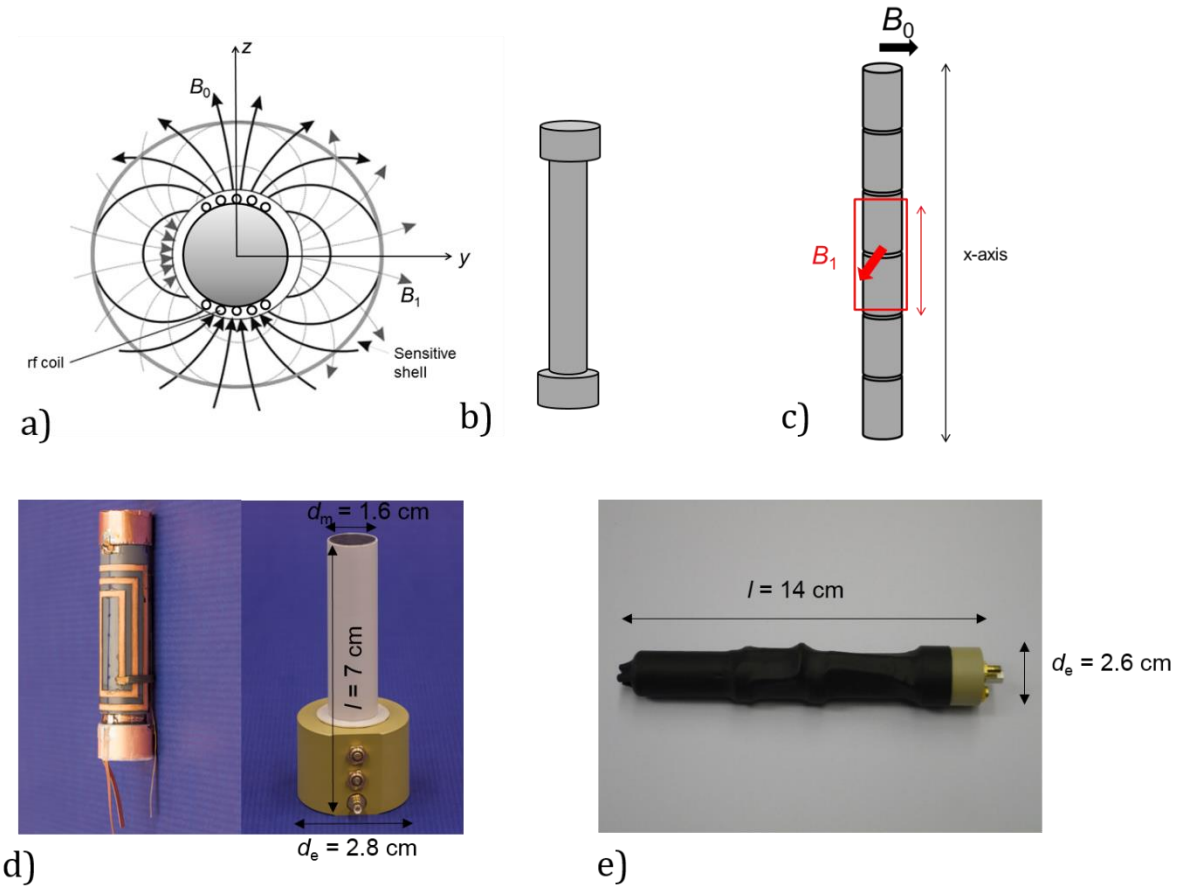

Fig. 6: a) Scheme of the NUMAR well logging sensor (adapted from [15]) and the Slim-Line-Logging tool [14,15]. The cylindrical magnet is polarized transverse to its long axis. With the use of a coil of five turns, a dipolar B_1 field is created perpendicular to the dipolar B_0 field. The condition of perpendicular B_0 and B_1 fields is fulfilled in a cylindrical shell, surrounding the magnet-coil assembly at a certain distance. b) Scheme of a the magnet assembly of a dumbbell shaped inside-out sensor as used in the Slim-Line-Logging tool and the DIP stick version I. The magnet caps at the ends of the sensor homogenize the magnetic field along the long axis of the sensor. The direction of the magnetic fields B_0 and B_1 is the same as for the scheme presented in c). c) Scheme of the DIP stick version II. This sensor is larger than the version shown in b) which compensates for the magnetic field homogeneity introduced by the dumbbell shape. d) Photograph of the magnet and coil assembly of the DIP stick version I (left). A photograph of a possible housing that protects the sensor from moisture and dimensions of the sensor. e) Photograph with size dimensions of the DIP stick version II. This sensor can be shifted through long cylindrical bore holes, since the electronic circuit has been reduced to the size of the sensor diameter.

3.2. Results and Discussion

The sensor has been constructed in two versions. The first version is of the same design as the Slim-line-logging sensor (named Version I in the following, see Fig. 6 b, d and Tab. 3), but smaller in size, whereas the latter version (named Version II in the following, see Fig. 6 c, e and Tab. 3) is larger and compensates the inhomogeneity effects, based on the dumbbell shape as used in Version I with greater length (Tab. 3) but better signal-to-noise ratio. The smaller version was used for moisture tracking in mortar joints between bricks in an old basement, while we investigated the second tool for laboratory experiments, such as drying experiments of lime-sand brick and aerated concrete as well as absorption experiments and cement curing.

3.2.1. Construction details

Both sensors have been constructed from NdFeB permanent magnets with N42 magnetization grade. Version I consists of a central magnet segment and two magnet caps with a slightly larger diameter are glued to the central segment. This results in a dumbbell shaped sensor with a polarization direction perpendicular to the long axis of the magnet. The radiofrequency coil of 4 cm length with five turns was fabricated by laser cutting of a 35 μm thin copper sheet. The main difference between the sensor versions I and II are the caps (Fig. 6 b, c). The magnet assembly of Version II consists of six single magnet segments with 1.8 cm diameter and 2 cm length. The repelling magnets are fixed with glue. The NMR circuit is reduced in size to match the diameter of the magnet assembly (Fig. 6 e) which enables depth profiling along long cylindrical holes. Both sensors are embedded in a polymer housing which protects the sensor from moisture. The DIP stick version II has a larger length/diameter ratio of 6.7 when compared to 4.4 for version I. This compensates for a potential loss of homogeneity (Fig. 7), while the NMR frequency could be increased from 3.6 to 10. 6 MHz and the measurement depth remains at a distance of 5 mm from the magnet surface (Fig. 7 a, b).

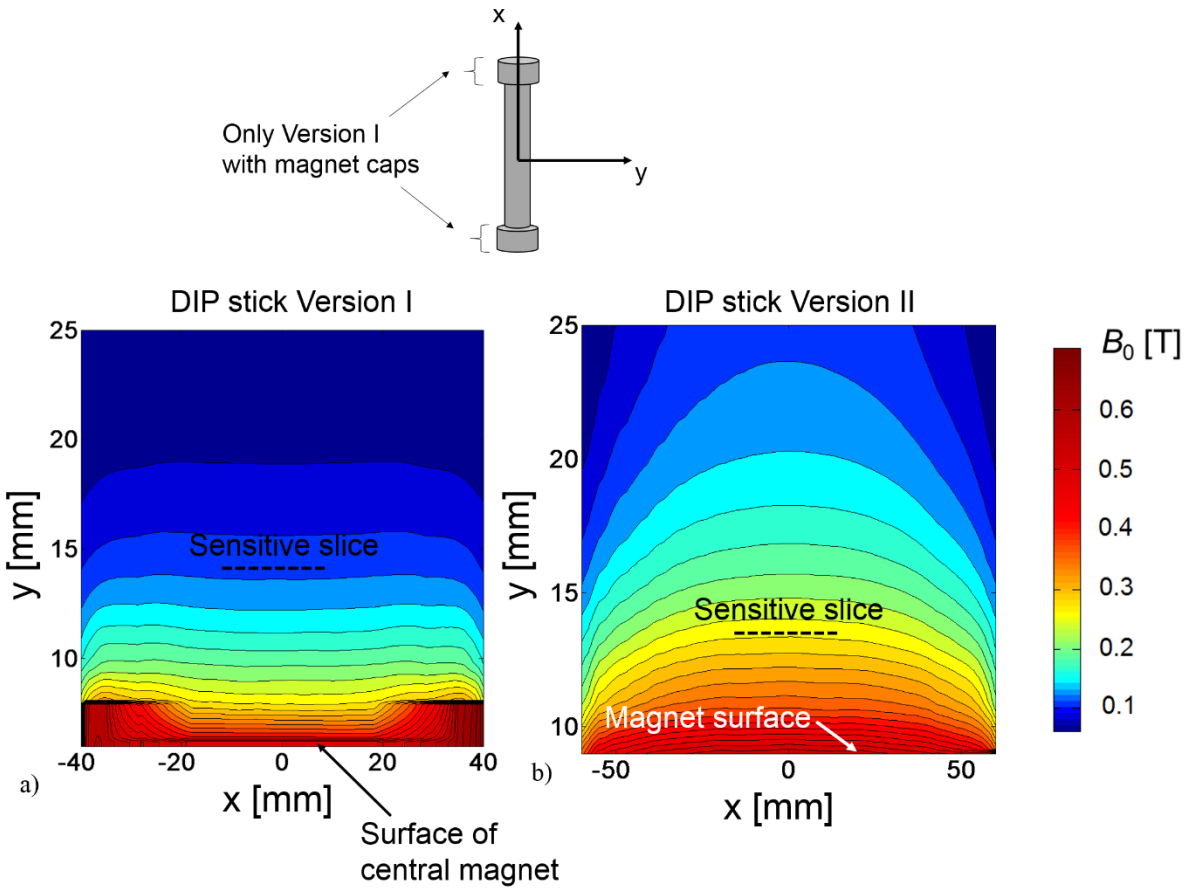

Fig. 7: Magnetic field simulations conducted with Opera 3D [21]. The origin of the *y*-axis of both graphs is located in the center of the magnet. The position of the magnet surface is indicated in the field map. a) Calculation of the static magnetic field B_0 along the long axis of the DIP stick version I with dumbbell shape. The sensitive slice is located at a NMR frequency of 3.6 MHz. b) Calculation of the static magnetic field B_0 along the long axis of the DIP stick version II. The sensor is elongated along its long axis when compared to version I and simulated without magnet caps at the ends of the sensor. The homogeneity is kept at a comparable level, whereas the NMR frequency could be increased to 10.6 MHz without losing measurement depth.

This results in a gain of sensitivity, since it is directly proportional to the NMR frequency. Another remarkable difference is the drastically reduced echo time. The coil geometry as well as the number of turns were the same as in version I. In version II copper wire of 1 mm diameter was used instead of thin copper sheets. The quality factors of the coils are 16.0 for version I and 27.9 for version II. Generally a higher quality factor correlates with longer ringing. In our case the reduction of magneto-acoustic ringing effects seems to be the major impact that enables the echo time reduction. The coil made of wire in version II was wound from one piece and it was mechanically easier to tightly fix on the plastic spacer. The thin coil of copper sheet (version I) was made of two pieces (2 turns and 3 turns) and combined with a connector. These additional solder points and a lower mechanical stability might be the main reasons that give rise to the longer echo times within CPMG echo trains. A shorter echo time is of benefit when analyzing porous building materials, to better resolve relatively dry building materials with fast relaxation.

Tab. 3: Comparison of two different DIP stick versions with specifications. Version I refers to a dumbbell shaped version, while Version II is a sensor without magnet caps at its ends, but elongated along the long axis.

Property	DIP stick Version I	DIP stick Version II
Frequency [MHz]	3.6	10.6
Gradient [T/m]	11.9	13.6
Min. echo time [µs]	250	80
Pulse length [µs]	46	14
Length [cm]	7	12
Diameter [cm]	1.6	1.8
Measurement depth [mm]	5	5

3.2.2. Field measurements

3.2.2.1. Measurements in an old basement

The sensor of version I has been applied to measure moisture in mortar joins between bricks in an old basement located in Schwalmtal, Northrine Westphalia, Germany (Fig. 8 a, b). The location studied was the basement of the administration building of the local church. We measured two positions located on different walls. One wall is close to a local river and is known to hold a higher moisture content than the other. We drilled holes of 1.6 cm diameter and used the DIP stick sensor to perform CPMG experiments (Fig. 1 b, c). Each experiment was repeated four times to check for reproducibility.

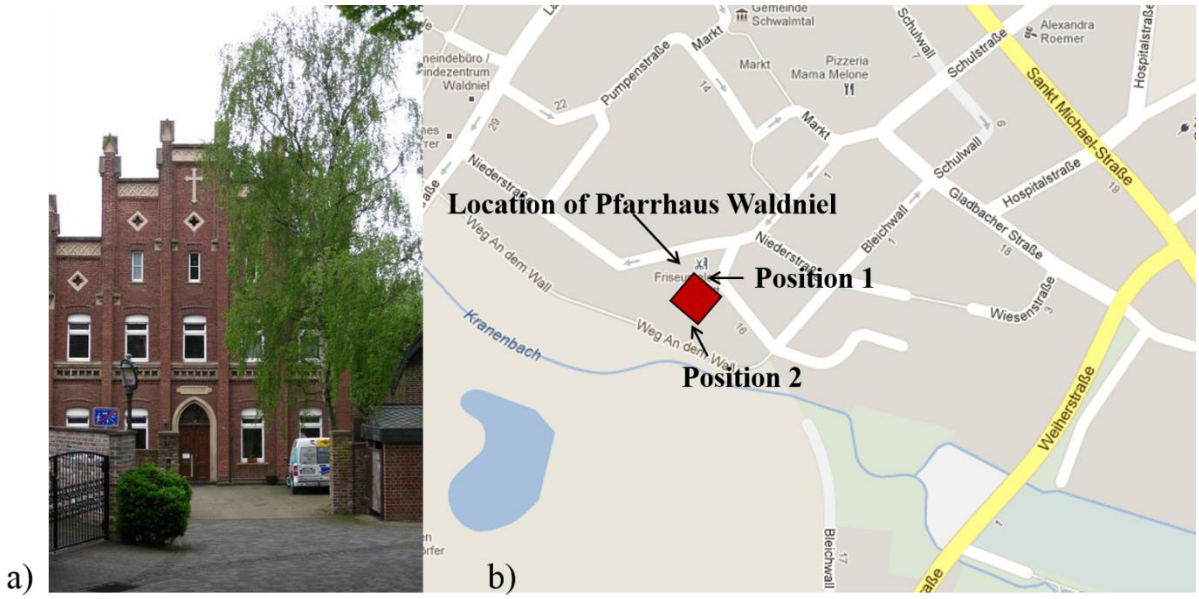

Fig. 8: a) Photograph of the old administration building of the local church St. Michael in Schwalmtal, Germany. We measured mortar joints between red bricks in the basement of the old house. b) Two positions were measured.

One position was located on a wall with direction to the city center whereas the other wall was located close to the local river. The wall of this position (Position 2) is known to contain more moisture.

All experiments were conducted with a KEA spectrometer from Magritek, at an NMR frequency of 3.6 MHz, with an echo time of 250 μs, a recycle delay of 1 s and 256 scans. Position 2 showed a 22.5 % higher moisture content than Position 1, calculated from the sum first two echoes from CPMG data normalized over four measurements (Fig. 9 b,c) and referenced to pure water.

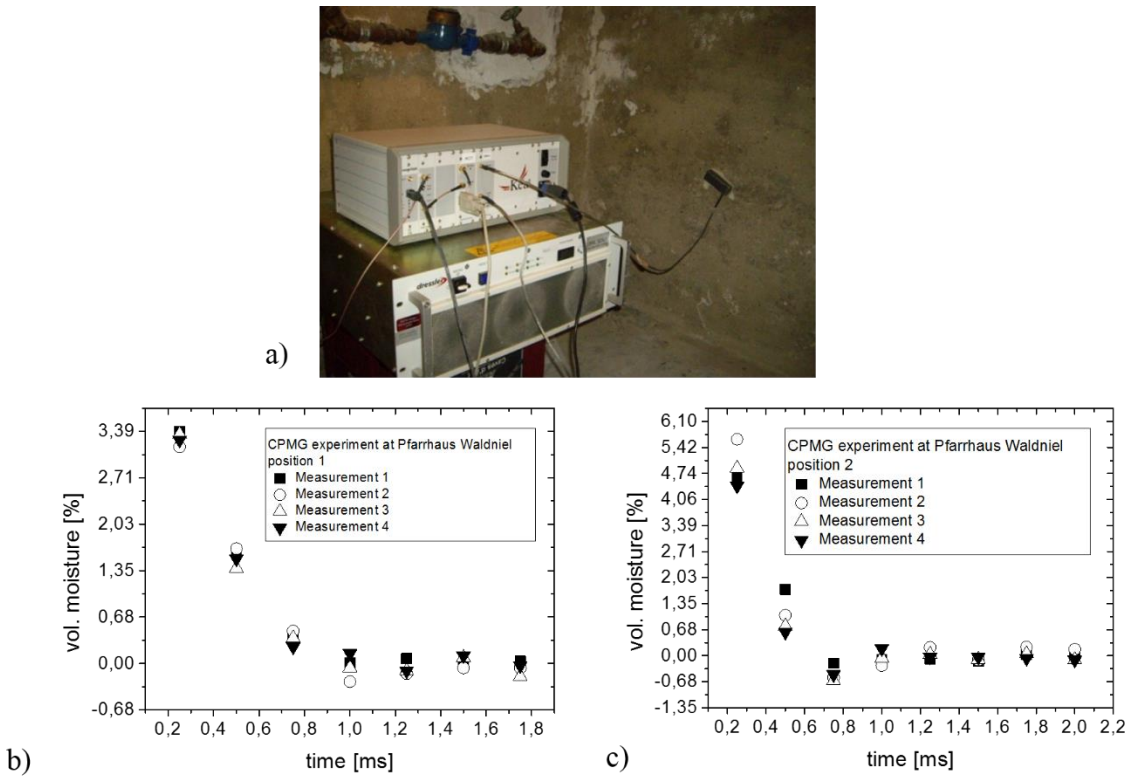

Fig. 9: a) Photograph of the measurement set-up in the basement of an old house in Schwalmtal, Germany. The position shown is referred to as position 1 in Fig. 8 b. b) CPMG data, measured at position 1. The measurement was repeated four times. c) CPMG data, measured at position 2. The measurement was repeated four times.

3.2.2.2. Measurements at the Aachen cathedral

Moisture measurements at the Aachen cathedral ("Aachener Dom") were conducted with the DIP stick tool version II. The statue shown in Fig. 10 was measured from the front side (often exposed to rain) and from the backside (not exposed to rain). The measurements were unfortunately done on a day after a very long period of warm temperatures and consequently the stone material seemed to be really dry. Without any treatment of the stone, no signal could be obtained. In a study before, signal was obtained, but in low quality due to sensor imperfections. Therefore, we decided to spray water onto the surface of the stone and then

measure the signal to analyze the effect of regular rain exposure to the pore structure by inverse Laplace transformation the CPMG signal decay.

The CPMG echo decay measured at position 1 (rain side) after spraying with water is shown in Fig. 10 b and shows NMR signal in good quality compared to the conditions (noise, low frequency). The CPMG echo decays of both measurement positions were inverse Laplace transformed and the distributions of relaxation times (related to pore-size-distribution) are shown in Fig. 10 c. They show that the stone from the front and the back of the statue consist of the same main pore size (peaks with highest intensity at approximately the same T_{2eff} values). The rain exposure seems to lead to another broad peak with higher relaxation times, which refers to larger pore-sizes with a broad distribution. This can be explained by out washing of the stone from the rain. The second peak of the back side shows smaller T_{2eff} values and consequently consists of smaller pores. This can be due to the fact that this side of the statue is less exposed to rain water ingress. These measurements demonstrate that the DIP stick sensor can be used in practical scenarios to monitor moisture in building structures.

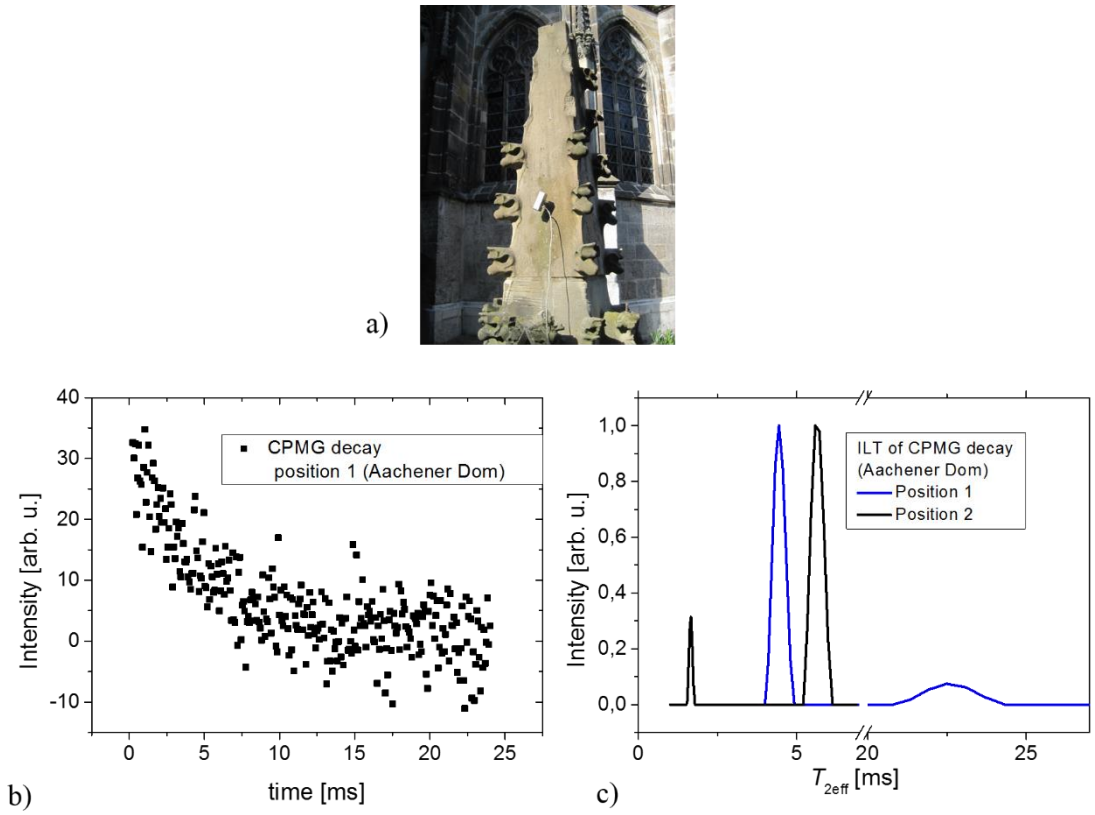

Fig. 10: a) Measurement set-up and position of the monument at the Aachener Dom. The measurement position shown in the picture is referred as position 1 in the following. This measurement position is regularly exposed to rain. Also measurements on the backside of the monument were conducted. b) CPMG echo decay, measured at position 1 which is commonly exposed to rain. c) Inverse Laplace Transformation of CPMG echo decays of two different measurement positions.

3.2.3. Laboratory measurements

All laboratory experiments were conducted with the DIP stick Version II at an NMR frequency of 10.6 MHz and a pulse length of 14 μs and a KEA II spectrometer from Magritek. For all experiments, the drilled holes were sealed with a laminated foil with the outer diameter tightly fitting to the diameter of the bore hole, to avoid evaporation through the bore-hole.

3.2.3.1. One-dimensional absorption and follow up drying of aerated concrete

We monitored moisture absorption of a block of aerated concrete (42 × 22.5 × 14 cm^3) mainly influenced through capillary transport. The aerated concrete-block was placed in a water tank, with a water pressure head of 2 cm, which was kept at a constant level. All sides, besides the top and bottom part of the concrete block were sealed with water resistant tape to limit moisture evaporation to one-dimension (Fig. 11 a). We recorded CPMG data with the DIP stick version II, positioned in a hole drilled at the center of the block and measuring the signal at a depth of 33.5 cm from the top, with a recycle delay of 0.8 s and 400 echoes for a time of 164 hours. The absorption and the drying processes can be depicted when plotting the initial signal amplitude of the CPMG decay versus the square root of time. As can be seen from Fig. 11 b, the absorption and the drying processes can both be divided into two stages, corresponding to two different pore-sizes which mainly contribute to the pore-size distribution. Aerated concrete is known to be a construction material, consisting of large aeration pores and smaller matrix pores [22]. Ioannou et al. showed a two stage absorption behavior of autoclaved aerated concrete with n-decane [22], where moisture absorption to the larger pores occurs in the first stage, followed by absorption into the smaller pores. Our results support this model, although the absorption speed deviates due to a different sample sizes and a different absorbate (water). In our case, the first absorption stage ends after a time of 19 h, and is followed by stage two absorption until we stopped the absorption experiment by removing the water reservoir at a time of 66 h. The follow up drying process can also be differentiated into two drying stages. The first drying stage is mainly affected by a continuous liquid moisture transport from the bulk material to the drying surface. This process is characterized by a relatively fast mass transport. Stage I drying follows up to a time of 105 h followed by stage II drying. Stage II drying occurs, when the evaporation rate becomes larger than the liquid transport rate from the bulk material [23]. The drying speed is significantly decreased. This experiment shows the potential of the DIP stick sensor to systematically study moisture dynamics in building materials and on construction sites.

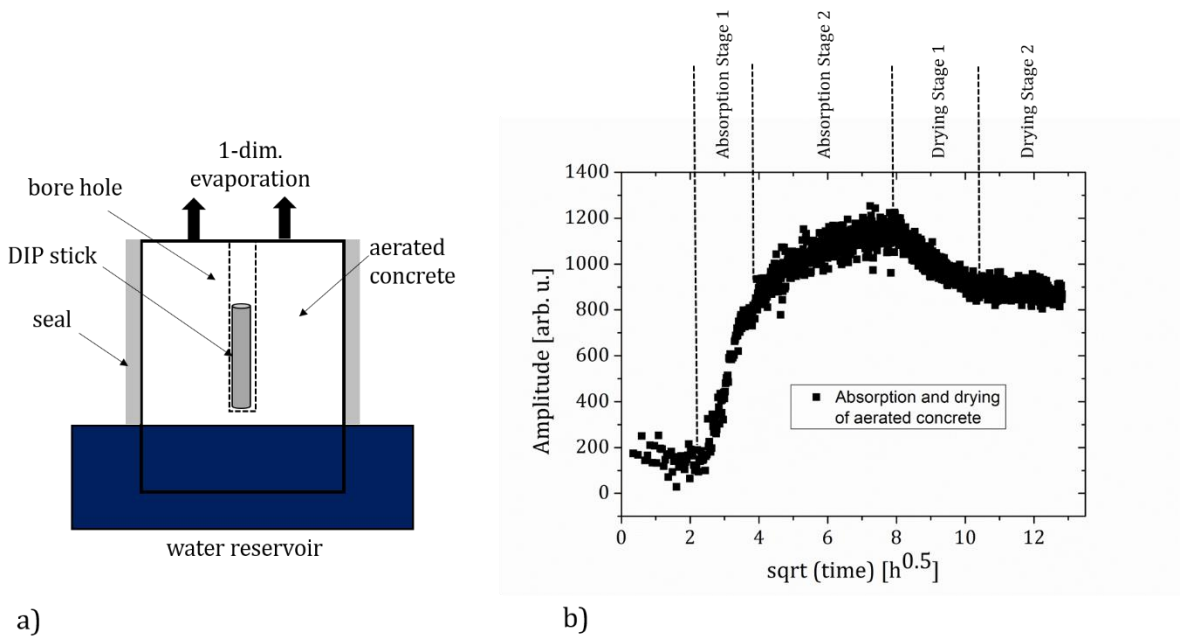

Fig. 11: a) Scheme of a laboratory water suction experiment, limited to one-dimension. The DIP stick version II sensor is placed inside a cylindrical bore hole in a block of aerated concrete. The concrete block is placed in a water tank with a water pressure head of 2 cm, kept at a constant level. All sides except for the top and the bottom of the stone are sealed to limit moisture evaporation to one-dimension. b) Initial amplitude of CPMG data, monitored during the absorption and drying processes. The absorption and the drying processes can be divided in different stages.

3.2.3.2. Curing of Cement

The curing process of cement pastes and concrete was tracked by inserting the DIP stick tool into fresh cement pastes and concrete blocks. CPMG echo trains were continuously recorded with curing time. Both the signal amplitude (Fig. 12 a) and the T_{2eff} values (Fig. 12 b) can be related to the curing process. The signal amplitude is a critical parameter in data analysis, as it can either represent the spin density (when integrating the initial echoes of the CPMG echo train) or a mean transverse relaxation time T_{2mean} (when integrating the complete echo train). The latter effect is shown in Fig. 12 b, where the mean relaxation time T_{2mean} (filled triangles) and the T_{2eff} values from a mono-exponential fit (open triangles) reflect the same shape of the curing curve. This intends the mean relaxation time to be less sensitive to noise than T_2 values extracted from exponential fits. Furthermore, it accurately describes the curing process of cement in terms of transverse relaxation. The mixture of cement, sand and water is commonly named “concrete”. Cement and water mixtures are commonly named “cement” or “cement paste” [24]. The cement pastes and the concrete sample were prepared following the recommended procedure of the manufacturer and varying the water-cement ratio (w/c). The impact of sand addtion can clearly be seen in Fig. 12 a. The mixture of sand and the cement has a stronger binding effect to water than the cement paste without additional sand. This is

reflected in a higher water concentration after a curing time of 12 h, as shown in the curing curve (Fig. 12 a, open triangles), than for the specimens without sand. The two cement samples without additional sand show a similar curing behavior, but can be distinguished in terms of the NMR amplitude, reflecting the water content (Fig. 12 a, Fig. 13 a) and curing speed (Fig. 13 a, b).

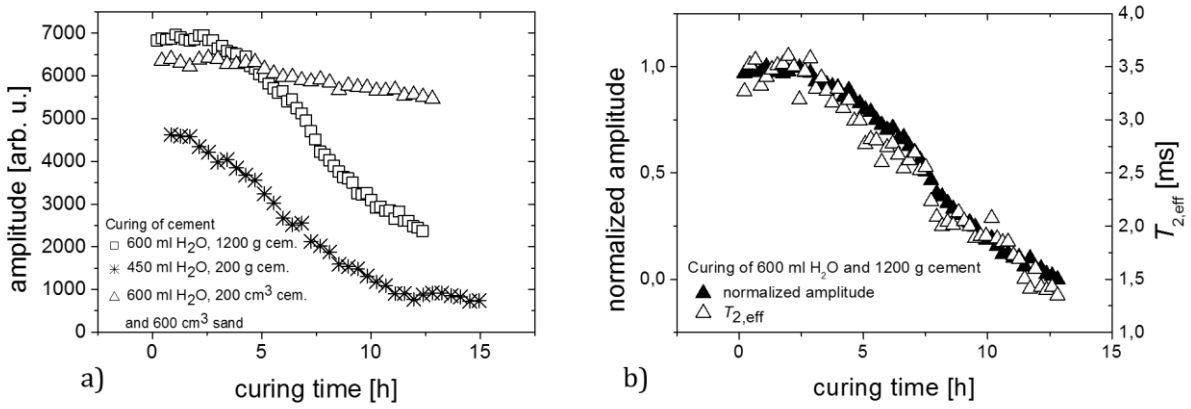

Fig. 12. a) Curing of cement pastes of varying w/c ratios and concrete, followed with the DIP stick. Each data point represents the mean relaxation time, calculated by integration of the complete echo train. b) The mean relaxation time, or simply amplitude (filled triangles) and the transverse relaxation times (open triangles) extracted from mono-exponential fits of CPMG echo trains, reveal the same information about the curing process. Both curves decrease over time due to the consumption of water and the change of the molecular mobility within the chemical reactions of the curing process. Data extracted from mono-exponential fits are more sensitive to noise.

The curing speed can either be evaluated in terms of the mean relaxation time or in terms of spin density. The curing process of cement pastes can be divided into different stages [24]. The first stage is mainly influenced by free water and lasts for about 15 minutes, which was not resolved in our experiments. The second stage is reported to be relatively short (1-2 hours in [24]) and characterized by only a slight change in T_2 and spin density. This so called 'dormancy period' [24] shows a certain mobility and allows to apply and process the cement paste. It is followed by a stage of a relatively large reduction of T_2 and a constant spin density (Stage III, Fig. 13 b), representing the hydration reaction to be the dominant mechanism. In case of different water-cement ratios, both stages last longer for the w/c ratio of 0.5 than for a w/c ratio of 0.375, which is in agreement with measurements performed by B. Manz et al. using the NMR-MOLE [24]. It is moreover possible to distinguish this curing-delay for higher w/c ratios by analysis of the T_2 weighted amplitude curves. Therefore the curing curves were fitted with a Gaussian fit function (Fig. 12 c) to compare the curing speeds. The fit shows a FWHM/2 value of 6.2 h for the cement sample containing 600 mL water (water-cement ratio, w/c = 0.5) and a FWHM/2 value of 5.5 h for the cement sample containing 450 mL water (w/c = 0.375), which

is in agreement by a delay of approximately 2 h shown in the spin density curing curves (Fig. 13 b).

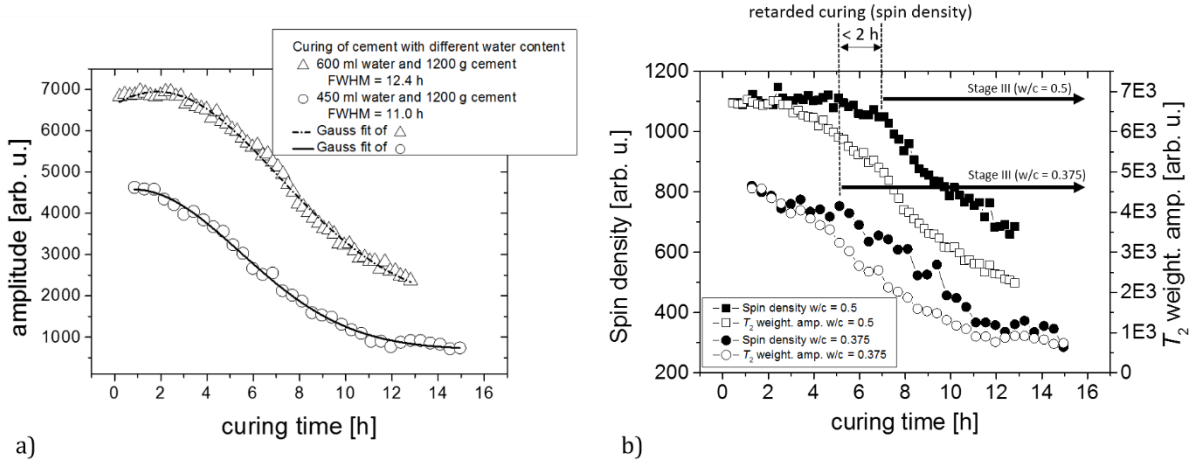

Fig. 13. a) Curing of cement samples of different initial water contents over time. The curing curves were fitted with a Gaussian function and show faster curing for the sample containing lower initial water content. A higher water amount seems to slow down the curing reaction. b) .

4. Conclusion

Miniaturization of NMR sensors enables applications where portability and flexibility are in demand, while it minimizes production costs and reduces problems with magnet storage and shielding. We drastically reduced the size of the NMR-MOUSE without losing sensitivity. The possibility of using small echo times within the Micro-MOUSE improves the quality of the data and the accuracy of the analysis of the fast relaxing signal components. We showed the advantages the Micro-MOUSE when analyzing drying processes of paint.

Miniaturization of inside-out NMR sensors also provides new opportunities for applying NMR in civil engineering, since it enables minimal invasive moisture tracking at construction sites or in laboratory. We presented a new and miniaturized NMR sensor of the inside-out type adapted from the geometry of the NUMAR well-logging sensor and the Slim-Line-Logging tool. The sensor was successfully applied in field and laboratory experiments. We analyzed static moisture content in the basement of an old house and a monument next to the Aachen cathedral. Moreover we studied the absorption and drying processes of aerated concrete as well as the curing process of cement in the laboratory.

Acknowledgement

We thank Andreas Janssen from Fraunhofer Institut für Produktionstechnologie (IPT) Aachen for supporting the coil production. Moreover we are grateful for the opportunity to measure in the basement of the administration building of St. Michael Waldniel, Schwalmtal, Germany. We thank the group of Prof. Mokwa and Dr. Schnakenberg (IWE, RWTH Aachen) for supplying the micro structured rf coil. We thank Helmut Maintz for the possibility of performing measurements at the Aachen cathedral and we acknowledge Deutsche Forschungsgemeinschaft (DFG, project: “Mikrosynergiespulen”) for financial support.

References

[1] B. Blümich, Essential NMR for Scientists and Engineers, Springer, Heidelberg, 2005.

[2] E. Danieli, J. Perlo, B. Blümich, F. Casanova, Angew. Chem. Int. Ed. 49 (2010) 4133-4135.

[3] R. K. Cooper, J. A. Jackson, Journal of Magnetic Resonance 41(1980) 400-405.

[4] L. J. Burnett, J. A. Jackson, Journal of Magnetic Resonance 41 (1980) 406-410.

[5] Z. Taicher, G. Coates, Y. Gitartz, L. Berman, Magnetic Resonance Imaging 12 (1994) 285-289.

[6] R. L. Kleinberg, A. Sezginer, D. D. Griffin, Journal of Magnetic Resonance 97 (1992) 466-485.

[7] F. Casanova, J. Perlo, B. Blümich, Single-Sided NMR, Springer, Heidelberg, 2011.

[8] V. Demas, P. J. Prado, Concepts in Magnetic Resonance Part A 34A, (2009) 48-59.

[9] B. Blümich, Scientific American, 299 (2008) 68-73.

[10] S. S. Zalesskiy, E. Danieli, B. Blümich, V. P. Ananikov, Chemical Reviews (2014).

[11] P.F. de J. Cano-Barrita, A.E. Marble, B.J. Balcom, J.C. García, I.V. Masthikin, M.D.A. Thomas, T.W. Bremner, Cement and Concrete Research 39 (2009) 324-328.

[12] W. M. Healy, ASHRAE Transactions 109 (2003) 232-242.

[13] J. Watzlaw, S. Glöggler, B. Blümich, W. Mokwa, U. Schnakenberg, Journal of Magnetic Resonance 230 (2013) 176-185.

[14] O. Sucre, A. Pohlmeier, A. Miniere, B. Blümich, Journal of Hydrology 406 (2011) 30-38.

[15] J. Perlo, E. Danieli, J. Perlo, B. Blümich, F. Casanova, , Journal of Magnetic Resonance 233 (2013) 74-79.

[16] G. Eidmann, R. Savelsberg, P. Blümler, B. Blümich, Journal of Magnetic Resonance A 122 (1996) 104-109.

[17] S. Anferova, V. Anferov, M. Adams, P. Blümler, N. Routley, K. Hailu, K. Kupferschläger, M.J.D. Mallett, G. Schroeder, S. Sharma, B. Blümich, Concepts Magn. Reson. 15 (2002) 15-25.

[18] M. van Landeghem, E. Danieli, J. Perlo, B. Blümich, F. Casanova, Journal of Magnetic Resonance 215 (2012) 74-84.

[19] E. Danieli, B. Blümich, Journal of Magnetic Resonance 229 (2013) 142-154.

[20] C. H. Hare, Paint Film Degradation: Mechanisms and Control, SSPC, 2001.

[21] Opera 3D, Vector Fields Limited, Version 8.0, 2001.

[22] I. Ioannou, A. Hamilton, C. Hall, Cement and Concrete Research 38 (2008) 766-771.

[23] G. H. A. van der Heijden, H. P. Huinink, L. Pel, K. Kopinga, Chemical Engineering Science 64 (2009) 3010-3018.

[24] B. Manz, A. Coy, R. Dykstra, C. D. Eccles, M. W. Hunter, B. J. Parkinson, P. T. Callaghan, Journal of Magnetic Resonance 183 (2006) 25-31.